J Solid State Electrochem (2012) 16:2941–2947
DOI 10.1007/s10008-012-1726-3

ORIGINAL PAPER

The effect of activation technology on the electrochemical performance of calcium carbide skeleton carbon

Hao Wu · Xianyou Wang · Xingyan Wang · Xiaoyan Zhang · Lanlan Jiang · Benan Hu · Yingping Wang

Received: 3 February 2012 / Revised: 12 February 2012 / Accepted: 12 March 2012 / Published online: 29 March 2012

Abstract Porous CaC_2-derived carbon (CCDC) was synthesized by one-step route from CaC_2 in a freshly prepared chlorine environment at lower temperature. As-prepared CCDC was activated by H_3PO_4, $ZnCl_2$, and KOH, respectively. The effects of the activation technology on the structure and morphology of CCDC were studied by X-ray diffraction, physical N_2 adsorption/desorption, and transmission electron microscopy. It has been found that the pore structure and specific surface area of CCDC are apparently improved after activation; the CCDC activated by KOH especially showed an excellent specific surface area of 1,100 $m^2\ g^{-1}$. The electrochemical performance of supercapacitors using activated CCDC as electrode active material was studied by cyclic voltammery, galvanostatic charge/discharge, and cycle life measurements. The results indicated that the CCDCs activated by H_3PO_4, $ZnCl_2$, and KOH revealed enhanced capacitances of 172.6, 198.1, and 250.1 $F g^{-1}$ in 6 M KOH electrolyte, which were increased by 11.4, 27.8, and 61.2 % compared with the pristine CCDC (155 $F g^{-1}$), respectively. Furthermore, the supercapacitors using all activated CCDCs as electrode active material exhibited excellent cycle stability, and the specific capacitance for all activated CCDC samples had nearly no change after 5,000 cycles.

Keywords CCDC · Activation · Supercapacitors

Electronic supplementary material The online version of this article (doi:10.1007/s10008-012-1726-3) contains supplementary material, which is available to authorized users.

H. Wu · X. Wang (✉) · X. Wang · X. Zhang · L. Jiang · B. Hu · Y. Wang
School of Chemistry, Key Laboratory of Environmentally Friendly Chemistry and Applications of Ministry of Education,
Xiangtan University,
Xiangtan, Hunan 411105, China
e-mail: wxianyou@yahoo.com

Introduction

In the last few years, electrochemical supercapacitors have drawn increasing attention in the field of electrochemical energy storage and conversion owing to their high power capability and long cycle life [1]. We can classify the supercapacitors into two types according to their energy storage mechanism, viz., redox supercapacitors and electrochemical double layer capacitors (EDLCs). EDLCs have emerged as a promising energy storage device for applications that need high power along with remarkable storage and cycle life [2]. As energy storage arises mainly from the accumulation of electronic and ionic charges at the interface between electrode materials and electrolyte solution in the EDLCs, the porosity and surface area of electrode active materials become the major factors that influence the specific capacitance of supercapacitors.

Because of carbon materials possessing high specific area, low cost , long cycle life, and wide use in aqueous and non-aqueous solvents [3, 4], various carbonaceous materials have been widely used as electrode materials for EDLCs, such as carbon nanotubes [5], carbon aerogels [6], and mesoporous carbon [7, 8] along with their mixture with metal oxides [9] or polymers [10]. During the recent years, a new class of nanoporous materials—carbide-derived carbon (CDC)—has been receiving attention in the literature for applications of EDLCs owing to their high specific surface area and fine-tuned pore size [11]. The skeleton carbon with network structures can be obtained by a temperature treatment of carbides in a containing chlorine atmosphere to selectively remove the metal (M) of the metal carbide (MC) and leave behind a porous carbon according to the following equation [12]:

$$MC + \frac{x}{2}Cl_2(g) \xrightarrow{400-1,200^{\circ}C} MCl_x + C(s) \quad (1)$$

CDC produced by halogenation of carbides exhibits a narrow pore size distribution, a tunable pore, and microstructure

by choosing the appropriate carbide precursor and chlorination temperature. However, the pore volume is limited by the amount of metal in the carbide structure, and variation of pore size by varying the process conditions is not possible for all carbides [13].

Our group has done some research about CCDC (CaC_2-derived carbon). Chunling Dai [14] developed a new type of one-step preparation technique for CCDC, which was synthesized from CaC_2 in a freshly prepared chlorine environment in the temperature range of 100–600 °C. Liping Zheng [15] prepared CCDC/polyaniline (PANI) composite materials by in situ chemical oxidation polymerization of an aniline solution containing well-dispersed CCDC; the CCDC/PANI composite electrode showed as high as the specific capacitance of 713.4 $F g^{-1}$ measured by cyclic voltammetry at 1 $mV s^{-1}$, but the capacitance retention of coin supercapacitor just remained at 80.1 % after 1,000 cycles. In fact, tuning the pore size is one of the most efficient ways to improve the specific capacitance and energy density of porous carbon materials [16]. Therefore, carbon post-treatments such as activation can usually be applied. Here, we report the chemical activation of CCDC with H_3PO_4, $ZnCl_2$, and KOH solution. The activated CCDCs were used as electrode active materials for supercapacitors. The supercapacitive characteristics were studied by cyclic voltammetry, galvanostatic charge/discharge, and cycle life measurements.

Experimental

Material synthesis

Synthesis of CCDC

All chemicals were of analytical grade and used without any further purification. The CCDC was prepared as follows: CaC_2 powder was placed in a quartz tube furnace, and the tube was Ar-purged for 30 min then heated to 400 °C. Freshly prepared chlorine gas was directly passed through the tube furnace once it reached the desired reaction temperature. After chlorination for 2 h, the furnace was naturally cooled down to room temperature under Ar purging. The resultant product was soaked in HCl solution (3 mol L^{-1}) and washed with distilled water later to remove further remainder. The acidic product was washed into neutral condition and then dried in a desiccator at 80 °C for 12 h.

Activation technologies of CCDC

H_3PO_4 activation

First, 1 g of CCDC sample was immersed in 100 g aqueous solution of chemical agents H_3PO_4 (30 wt.%) at room temperature. Second, the temperature was increased to 85 °C and then the sample was exposed in this temperature for 3 h. It was then cooled down to ambient temperature and left at rest for 12 h. After the above treatment, the mixture was washed and filtrated with distilled water until the pH of the filtrate water became neutral. Lastly, it was dried at 110 °C for 12 h to obtain CCDC–H_3PO_4.

$ZnCl_2$ activation

The resultant CCDC sample was soaked in $ZnCl_2$ solution (0.37 mol L^{-1}) and stirred in 80 °C for 7 h then filtrated and dried at 80 °C for 12 h. The filtered product was placed in a quartz tube furnace, and the tube was Ar-purged for 30 min then heated to 600 °C. The product was soaked in diluted hydrochloric acid, heated to 90 °C and stirred for 30 min, and then washed with distilled water until the pH of filtrate water became neutral. The filtered product was dried at 80 °C for 12 h. This product was named CCDC–$ZnCl_2$.

KOH activation

The mass ratio of KOH to CCDC was 5:1. After being impregnated for 12 h, the mixtures were heated at 110 °C in an oven to remove the water. Then, the dried materials were activated at 900 °C for 1 h under Ar flow. Once cooled down, the resultant samples were impregnated in enough 2 MHCl solution for a few hours and later washed with a great deal of deionized water to remove K^+ and Cl^-. The washed samples were dried at 110 °C for 12 h to obtain the finally activated CCDC– KOH product.

Preparation of electrode and coin supercapacitor assembly

The mass ratio of CCDC/acetylene black was 8:1. The powder mixture was mixed with 10 wt.% of polyvinylidene fluoride aqueous suspension as a binder to obtain a paste. The paste was then pressed into the nickel foam substrate using a spatula. After drying in vacuum at 110 °C for 12 h, the electrode of nickel foam was pressed at 15 MPa for 1 min to assure good electronic contact and to form a circular tablet (diameter= 1.4 cm). Symmetrical coin supercapacitors were constructed with 6 M KOH electrolyte, in which two primitive CCDC or activated CCDC electrodes were separated by a separator of electrode/separator/electrode order. Then, the supercapacitors were sealed using a packing machine.

Characterization of the materials

Transmission electron microscopy (TEM) measurements were performed using a FEI Tecnai G2 microscope at 200 kV. X-ray diffraction (XRD) analysis was done using a diffractometer (D/MAX-3 C) with CuKα radiation (λ=

1.5406 Å) and a graphite monochromator at 40 kV and 300 mA. The carbon also was characterized by physical N_2 adsorption/desorption at 77 K (using an AUTOSORB-1 instrument from Quantachrome). The specific surfaces (SBET) were derived from N_2 adsorption isotherms by means of the BET equation. The pore size distributions and medium pore diameter were determined using the BJH method. The micropore volume (V_{micro}) was obtained by the Dubinin–Raduskevich equation and the total volume of porous (V_{total}) by Gurvitsch rule at $P/P_0 \approx 0.985$.

Electrochemical measurements

The electrochemical performance of the electrodes was characterized by cyclic voltammetry (CV), galvanostatic charge/discharge, and cycle life measurements. The experiments were carried out using a three-electrode system, in which nickel foam and the Hg/HgO electrode were used as counter and reference electrodes, respectively. The electrolyte used was 6 M KOH solution. The charge/discharge and the cycle life measurements at constant current were carried out by potentiostat/galvanostat on button cell supercapacitors.

Results and discussion

Material characterization

N_2 adsorption isotherms were measured to determine the specific surface area and pore size distribution of CCDC. As shown in Fig. 1a, the N_2 adsorption/desorption isotherm of the pristine CCDC is close to type-I, indicating that the pristine CCDC shows mainly microporous characteristics. The isotherm of CCDC–$ZnCl_2$ shows a small hysteresis loop at medium relative pressure, which is due to the presence of mesopores in the carbon framework. The N_2 adsorption/desorption isotherm of CCDC–KOH is a typical type IV curve and shows an obvious capillary condensation step (hysteresis loop) at medium relative pressure, which indicates that the mesopores have been shaped after KOH activation. The pore structure parameters of the pristine CCDC and activated CCDC samples are all listed in Table 1. For CCDC–KOH, the V_{micro}/V_{total} is 18 %, indicating that it is close to an absolute mesoporous structure. In the case of CCDC–$ZnCl_2$, the V_{micro}/V_{total} is 37 %, which is in accordance with the result presented in Fig. 1b. Therefore, CCDC–$ZnCl_2$ has some mesopores besides the large amounts of micropores. Besides, the CCDC–KOH shows much higher BET surface area and larger pore volume of 1,100 $m^2\ g^{-1}$ and 1.74 $cm^3\ g^{-1}$ (increased from 336 $m^2\ g^{-1}$ and 0.46 $cm^3\ g^{-1}$), respectively, which can be attributed to the corrosion of the CCDC micropore wall in KOH solution at high temperatures. The results of N_2 adsorption/desorption isotherms also confirm that the amount of

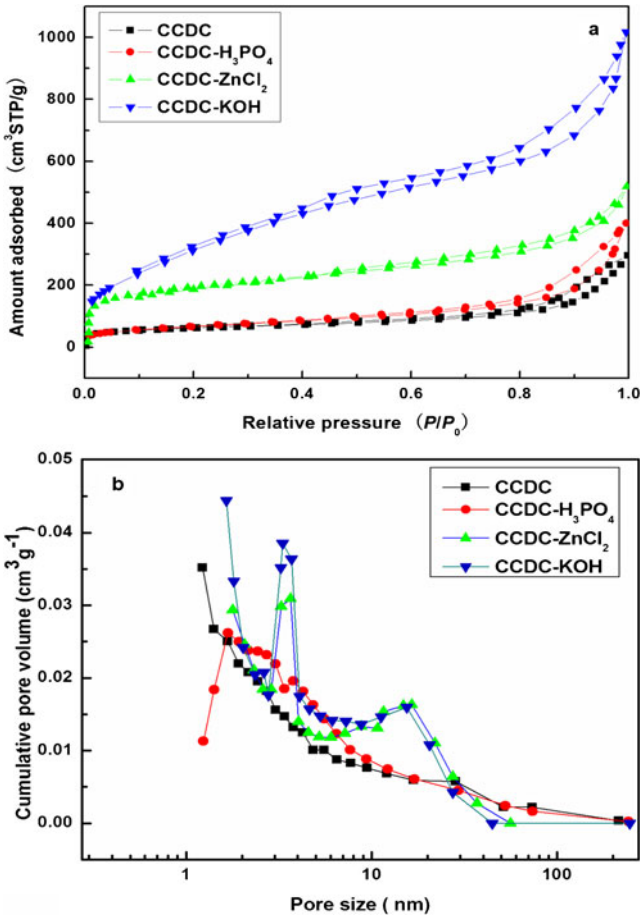

Fig. 1 **a** N_2 sorption isotherms of carbon samples and **b** pore size distribution calculated using the BJH method

micropores and mesopores of CCDC can be controlled by adjusting the activated method and the kinds of activating agent. As can also be seen in Fig. 2b, the mesopore surface area of CCDC increases gradually with the activation of CCDC, and CCDC–KOH has a relatively abundant mesopore surface area in the pore size range of 2–4 nm [17]. On the other hand, the N_2 adsorption/desorption isotherms of CCDC–H_3PO_4 are close to the pristine CCDC, thus indicating that the pore size distribution was scarcely changed after activation by H_3PO_4.

Table 1 Pore structure parameters of the pristine CCDC and activated CCDC

Samples	Surface area ($m^2\ g^{-1}$)		Pore size (nm)	Volume ($cm^3\ g^{-1}$)	
	S_{BET}	S_{micro}		V_{total}	V_{micro}
CCDC	336	120	1.80	0.46	0.33
CCDC–H_3PO_4	422	107	1.27	0.60	0.38
CCDC–$ZnCl_2$	706	153	7.23	0.81	0.30
CCDC–KOH	1100	200	8.83	1.74	0.17

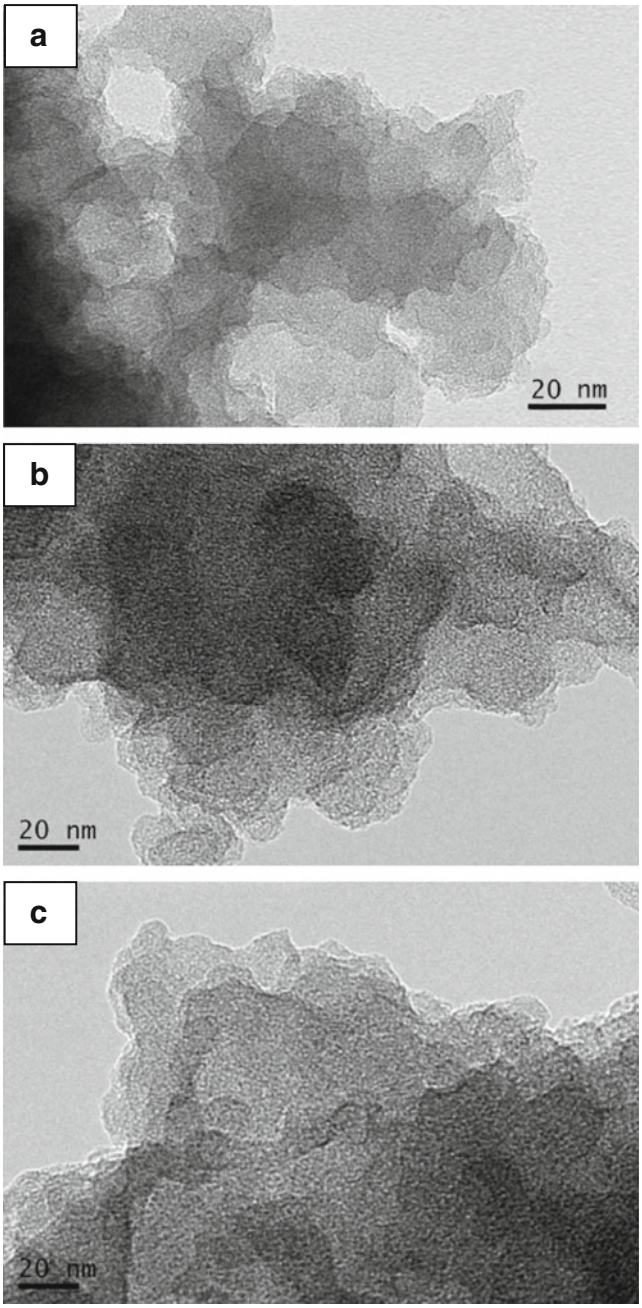

Fig. 2 TEM images of CCDC (**a**), CCDC–$ZnCl_2$ (**b**), and CCDC–KOH (**c**)

It can be seen in Table 1 that the BET surface area, mesopore surface area, and total pore volume of the CCDC increase gradually after activation. Particularly, the CCDC–KOH shows the highest BET surface area and total pore volume, which are as high as 1,100 $m^2\ g^{-1}$ and 1.74 $cm^3\ g^{-1}$, respectively, so KOH treatment is highly efficient for the activation of CCDC.

The microstructures and morphologies of the pristine CCDC, CCDC–$ZnCl_2$, and CCDC–KOH were examined by TEM. The typical results are shown in Fig. 2. As shown in Fig. 2a, the pristine CCDC consisted of completely amorphous carbon with no detectable graphene layers. The surface morphology of CCDC becomes salient and rough after being activated by KOH (Fig. 2b) and $ZnCl_2$ (Fig. 2c), suggesting the enlarging of micropores and increasing of the surface area. Therefore, the said results reveal that chemical activation using KOH for CCDC is favorable to expansion of the size of micropore.

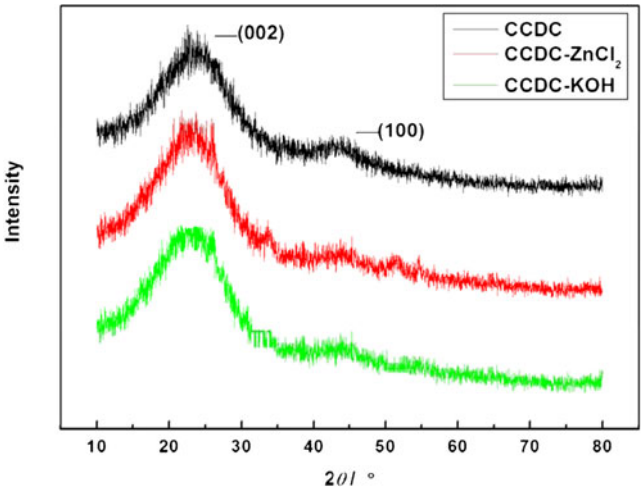

Fig. 3 XRD patterns of the pristine CCDC, CCDC–$ZnCl_2$, and CCDC–KOH

The XRD patterns of CCDC and activated CCDC are shown in Fig. 3. There are two broad diffraction peaks at around $2\theta=25^{o}$ and 44^{o} in each spectrum, corresponding to the diffraction of (002) and (100) of graphite, respectively. It indicates a highly disordered and amorphous structure of the CCDC derived from CaC_2. It was found that the peak (100) of CCDC–KOH at $2\theta=44°$ seemed to be inconspicuous, indicating no graphitization tendency in CCDC even after activation in 900 °C. The well-resolved diffraction peaks of CCDC–KOH were preserved after activation, indicating the

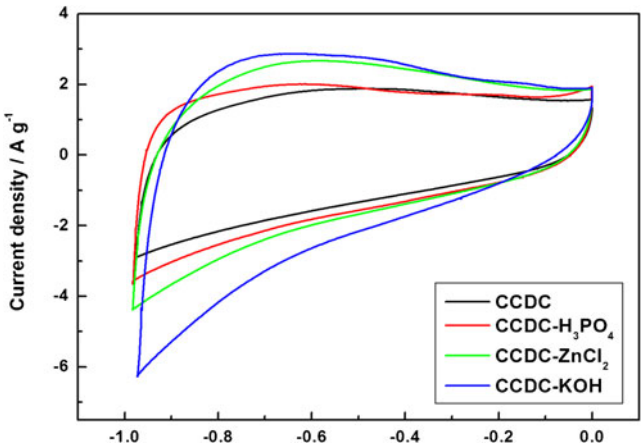

Fig. 4 Cyclic voltammograms of CCDC and activated CCDC electrodes (10 mV s^{-1})

Table 2 The specific capacitance of electrodes with different materials

Samples	Scan rate			
	1	2	5	10
CCDC	179.6	172.4	166.3	155.0
CCDC–H_3PO_4	211.6	201.6	184.2	172.6
CCDC–$ZnCl_2$	277.0	259.6	229.5	198.1
CCDC–KOH	280.1	273.5	265.2	250.1

main skeleton structure survived from the severe KOH activation [18].

Electrochemical test

To test the EDLCs performance of the pristine CCDC and activated CCDC, CV measurements were conducted. The CV profiles of all samples at a scan rate of 10 mV s^{-1} are displayed in Fig. 4. The CV profiles of pristine CCDC are of a standard rectangular shape, which shows good capacitive behavior. Of special interest is the fact that activated CCDCs still maintain good capacitive behavior at a higher sweep rate. Maybe due to the short diffusion distance from mesopores to micropores and the fast ionic transportation within the mesopores, the hierarchical porous structure helps to maintain good capacitive behavior at a higher sweep rate. The current response values of CCDC–KOH are higher than that of pristine CCDC, CCDC–H_3PO_4, and CCDC–$ZnCl_2$. It means that, even at higher scan rates, the affluent porous structure on the skeleton of CCDC–KOH remarkably promotes the formation of a double layer and contributes to fast ion diffusion into larger mesopores. The abundant mesopores derived from collapsed micropores make the diffusion resistance between the micropores and the main mesopore channel to increase, which results in other highly activated samples (CCDC–H_3PO_4 and CCDC–$ZnCl_2$) and inferior electrochemical performance.

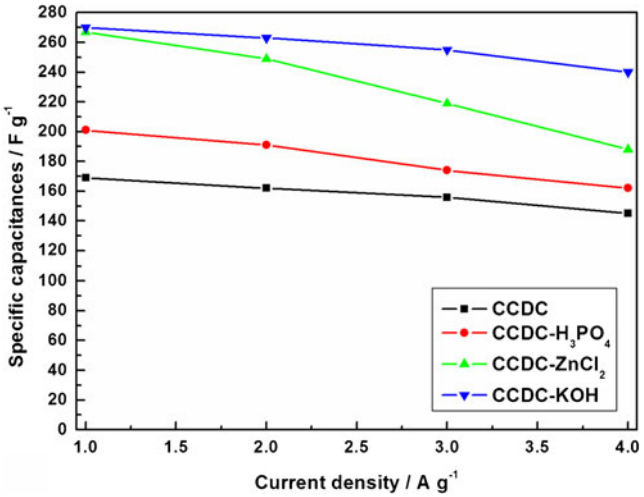

Fig. 6 Comparison of capacitance decay with increasing discharge current density for all CCDC samples

All data of specific capacitance are shown in Table 2, in which CCDC–KOH displays a higher specific capacitance than that of other materials. This is in good agreement with the cyclic voltammogram results.

Figure 5 displays the charge/discharge curves of the supercapacitors using pristine CCDC and activated CCDC samples as active materials, which are obtained at a current density of 1 A g^{-1}. The isosceles triangle curves of charge/discharge profiles indicate the simulative capacitor with the performance of electrochemical stability and reversibility. Galvanostatic charge/discharges with a current density of 1–5 A g^{-1} were conducted to calculate the specific capacitance

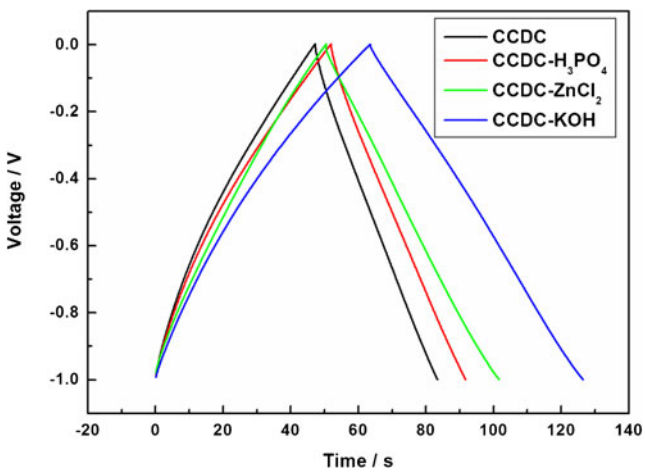

Fig. 5 Charge/discharge curves of primitive CCDC and activated CCDC at current density of 1 A g^{-1}

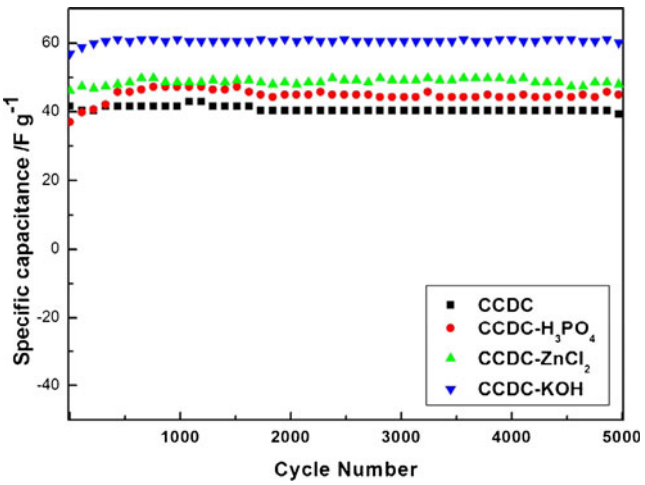

Fig. 7 The cycle life curve of pristine CCDC and activated CCDC supercapacitors at current density of 0.5 A g^{-1}

of all carbon samples. The corresponding specific capacitance values were calculated by the equation [19]:

$$C_{\text{single}} = \frac{4 \times I \times t}{\Delta V \times m} \quad (2)$$

where I is the discharge current (A), t is the total discharge time (s), m is the total mass of active material in both electrodes (g), ΔV is the potential difference during the discharge (V), and C_{single} is the single-electrode specific capacitance (F g^{-1}).

The obtained capacitance values of all carbons vs. current densities are displayed in Fig. 6. As the current increases, the specific capacitance of all samples drops slowly, which confirms that the ions have enough time to diffuse into the micropores of CCDC at a low current, while due to the steric limitations at high currents the ions can only partially penetrate into the micropores. However, all samples did not show violent capacitance losses with an increase of current load, and the specific capacitance of CCDC–KOH is obviously higher than that of others. The change in specific capacitance follows a degressive order: CCDC–KOH > CCDC–$ZnCl_2$ > CCDC–H_3PO_4 > CCDC. Apparently, the tendency of the change of the specific capacitance is the same as the degressive order of specific surface area and mesopore volume of CCDC samples listed in Table 1. This indicates that chemical activation of CCDC is a powerful way to improve electrical double-layer performance due to the increase of the specific surface area and mesopore volume [20]. Outstanding capacitance values have been obtained when CCDC–KOH with pore size larger than 2 nm, S_{BET} of around 1,100 m^2 g^{-1}, and V_{meso} below 2 cm^3 g^{-1} was used.

In order to research the cycle life of the said materials, the cycle life curves after 5,000 cycles for the supercapacitors using pristine CCDC and activated CCDC as electrodes at a current density of 0.5 A g^{-1} are given in Fig. 7. It can be seen from Fig. 7 that the cycle curve of the activated CCDC samples lies obviously higher than that of the pristine CCDC. That is because the specific capacitance of the EDLCs for activated CCDC samples is much larger than that of the pristine CCDC. Besides, all the specific capacitance values of supercapacitors are almost just one fourth of the data which were calculated from CV and galvanostatic charge/discharge measurements for a single electrode [21], and there are up trends in the cycle curves of the activated CCDC samples at the beginning cycles. Maybe more time is needed in several initial charging/discharging cycles to let the electrolyte completely enter into the pores of the electrode material [22]. This phenomenon is also frequently seen for a supercapacitor or a battery when the specific surface area of the electrode material is much larger. In a short, all results of the EDLCs based on the activated CCDC samples show good cycle performance. CCDC–KOH especially exhibits an optimum electrochemical capacitance characteristic.

Conclusions

The structure, morphology, characteristics of pore structure, specific capacitance, and cycle life of the CCDC samples based on pristine CCDC and activated CCDCs were compared systemically. The pristine CCDC and CCDC–H_3PO_4 showed mainly microporous characteristics. The CCDC–$ZnCl_2$ revealed some mesopores besides the large amounts of micropores, while CCDC–KOH was close to an absolute mesoporous structure. All the activated samples showed higher specific capacitance and good cycle performance. CCDC–KOH especially showed the largest surface area (1,100 m^2 g^{-1}) and mesopore volume (1.57 cm^3 g^{-1}). It obtained the highest specific capacitance of 250.1 Fg^{-1} at a scan rate of 10 mV s^{-1} and better rate capability in 6 M KOH electrolyte. The excellent capacitive behavior of CCDC–KOH may due to the high surface area, abundant micropores and mesopores, as well as moderate crystal structure [23].

References

1. Phatiphat T, Stephane R, Bernard D (2009) J Power Sources 193:376–385
2. Miller JR, Burke AF (2008) Interface 17:53–57
3. Simon P, Gogotsi Y (2008) Nat Mater 7:845–854
4. Burke A (2007) Electrochim Acta 53:1083–1091
5. Ci L, Manikoth SM, Li X, Vajtai R, Ajayan PM (2007) Adv Mater 19:3300–3303
6. Emmenegger Ch, Mauron Ph, Sudan P, Wenger P, Hermann V, Gallay R, Zuttel A (2003) J Power Sources 124:321–329
7. Fuertes AB, Lota G, Centeno TA, Frackowiak E (2005) Electrochim Acta 50:2799–2805
8. Ania CO, Khomenko V, Raymundo-Piñero E, Parra JB, Béguin F (2007) Adv Funct Mater 17:1828–1836
9. Huang QH, Wang XY, Li J (2006) Electrochim Acta 52:1758–1762
10. Kuhn P, Forget A, Su DS, Thomas A, Antonietti M (2008) J Am Chem Soc 130:13333–13337
11. Largeot C, Portet C, Chmiola J, Taberna PL, Gogotsi Y, Simon P (2008) J Am Chem Soc 130:2730–2731
12. Gogotsi Y, Nikitin A, Ye H, Zhou W, Fischer JE, Yi B, Foley HC, Barsoum MW (2003) Nat Mater 2:591–594
13. Schmirler M, Glenk F, Etzold Bastian JM (2011) Carbon 49:3679–3686
14. Dai CL, Wang XY, Wang Y, Li N, Wei JL (2008) Mater Chem Phys 112:461–465

15. Zheng LP, Wang Y, Wang XY, Li N, An HF, Chen HJ, Guo J (2010) J Power Sources 195:1747–1752
16. Barpanda P, Fanchini G, Amatucci GG (2011) Carbon 49:2538–2548
17. Sevilla M, Foulston R, Mokaya R (2010) Energy Environ Sci 3:223–227
18. Portet C, Kazachkin D, Osswald S, Gogotsi Y, Borguet E (2010) Thermochim Acta 497:137–142
19. Qu DY, Shi H (1998) J Power Sources 74:99–107
20. Xing W, Huang CC, Zhuo SP, Yuan X, Wang GQ, Hulicova-Jurcakova D, Yan ZF, Lu GQ (2009) Carbon 47:1715–1722
21. Jänes A, Kurig H, Lust E (2007) Carbon 45:1226–1233
22. Chen WC, Wen TC, Teng H (2003) Electrochim Acta 48:641–649
23. Zheng ZJ, Gao QM (2011) J Power Sources 196:1615–1619